Degradation modes of alkaline fuel cells and their components

Klaus Tomantschger and Robert Findlay
Battery Technologies Inc., 2480 Dunwin Drive, Mississauga, Ont. L5L 1J9 (Canada)

Michael Hanson
PPG Industries Inc., Glass R&D, P.O. Box 11472, Pittsburgh, PA 15238-0472 (USA)

Karl Kordesch
Technical University Graz, A-8010 Graz (Austria)

Supramaniam Srinivasan
Center for Electrochemical Systems and Hydrogen Research, Texas Engineering Experiment Station, The Texas A&M University System, College Station, TX 77843-3577 (USA)

(Received October 18, 1991; in revised form December 9, 1991)

Abstract

The performance and life-limiting parameters of multilayer polytetrafluoroethylene (PTFE) bonded carbon air cathodes and hydrogen anodes, developed at the Institute for Hydrogen Systems (IHS) for use in low temperature alkaline electrolyte fuel cells (AFC) and batteries, were investigated. Scanning electron microscopy (SEM), X-ray energy spectroscopy (XES), electron spectroscopy for chemical analysis (ESCA), microcalorimetry and intrusion porosimetry techniques in conjunction with electrochemical testing methods were used to characterize electrode components, electrodes and alkaline fuel cells. The lifetime of air cathodes is mainly limited by carbon corrosion and structural degradation, while that of hydrogen anodes is frequently limited by electrocatalyst problems and structural degradation. The PTFE binder was also found to degrade in both the cathodes and the anodes. The internal resistance, which was found to generally increase in AFCs in particular between the cathode and the current collector, can be minimized by the proper choice of materials. Temperature cycling of AFCs may result in mechanical problems; however, these problems can be overcome by using AFC components with compatible thermal expansion coefficients.

Introduction

General

In the 1970s and 1980s, major efforts were directed to develop alkaline fuel cells (AFC), specifically designed to overcome cost and performance limitations of fuel cells, for a broad range of applications. Despite the fact that they have to operate on clean hydrogen and scrubbed air, AFCs are strong candidates as power source for stationary applications, portable power generators and electric transportation because of compactness, low cost (using non-noble metal electrocatalysts), simplicity and reasonable life [1]. Since the early 1970s Elenco in Belgium has developed polytetrafluoroethylene (PTFE) bonded carbon electrodes. At the present time, the company has a projected production capability of 500,000 m^2 per year. Elenco's fuel cell system

0378-7753/92/$5.00

uses a circulating KOH electrolyte. A city bus with 10 kW_e AFC was built in the early 1980s. Forty kW_e systems have been developed since. Lifetimes of up to 20,000 operating hours have been reported on electrodes and in small stacks [2]. The most notable low cost AFC development efforts were those of Alstom Atlantique and Occidental which were started in 1978. The basic concept of these fuel cells is a low-cost, high-performance configuration which is economical, compact in size and easy to manufacture [3]. The cells use low-cost thermoplastic and conductive materials and thus avoid the use of expensive components and complex methods of assembly. Occidental demonstrated two 4.5 kW_e bipolar fuel cell stacks, operating with circulating sulfuric acid or KOH electrolyte, at the Fuel Cell Seminar in Tucson in 1985. Despite the advantages of low cost, simple construction and ease of mass production, the commercial effort has since been abandoned. The highest profile AFC is the 20 kW AFC power plant built by United Technologies Corporation (UTC) for the Space Shuttle orbiter, which exhibits an impressive performance [4]. In 1986 the European Space Agency (ESA) started the development of a reusable spacecraft for their agency's manned missions. The Hermes spacecraft will be equipped with a 4 kW AFC system as the main electrical power source and it will in addition supply drinking water for the crew. R&D efforts are aimed at the establishment of the most efficient, reliable and adequate technology for this purpose and are shared by various groups throughout Europe [5].

In Canada AFC activities were started at the Laboratory of Advanced Concepts in Energy Conversion (LACEC) group in 1979. After 1983 these efforts were continued by the Institute for Hydrogen Systems (IHS), which aimed at the development of low-cost portable AFC power sources for industrial and transportation applications [6]. The activities were split into two major tasks: (i) the development of high-performance low-cost gas diffusion electrodes for use in fuel cells and metal air batteries; (ii) fuel cell stack development. PTFE bonded multilayer carbon electrodes were the major focus of attention. The fuel cell stack development focused on the compact, low-cost bipolar design [7]. In 1987 the IHS technology was acquired by Battery Technologies Inc. (BTI).

Multilayer carbon electrodes and electrode design

Gas diffusion electrodes, developed at IHS, typically consist of three layers: the electrode backing, the gas diffusion layer and the electrocatalyst layer [6]. Multilayer gas diffusion electrodes not only serve as reaction zone for the fuel cell reaction but also provide pores for gas diffusion and barriers for the electrolyte entering the diffusion layer [8]. The structure has a great effect on the performance of the electrode. Using scanning electron microscopy (SEM) and intrusion porosimetry, it was shown that the PTFE bonded carbon multilayer gas diffusion electrodes can best be characterized by two components: a macrostructure and a microstructure [9]. The macrostructure, created by the partial enclosure of the carbon particles by the PTFE, provides the skeleton for the electrode, serves as current collector and is the mechanical support for the electrode. The electrode microstructure is created by the pore system of the carbon particles themselves. In the catalyst layer, the primary (macro) pore structure is responsible for the ionic transport while the secondary (micro) pore structure furnishes the gas transport. The electrochemical reactions proceed in the three-phase region, where the primary and secondary pore structures meet. Both the primary and secondary pore structure serve as the gas feed channels in the diffusion layer.

The platinum or metal oxide electrocatalyst is incorporated in the air cathode in the early stages of the electrode fabrication process. In the air cathode the electrocatalyst

is uniformly distributed throughout the entire electrocatalyst layer. Hydrogen electrodes are postcatalyzed with a mixture of palladium (Pd) and rhodium (Rh). Hydrogen anodes exhibit a higher concentration of electrocatalyst in the outer layer and have a decreasing content towards the center of the electrode. A comparison between pre- and postcatalyzation methods shows that electrodes which were postcatalyzed required a shorter break-in time to reach optimum electrode performance [10].

Lifetimes of over 3500 h were demonstrated on first generation electrodes at a nominal current density of 100 mA/cm^2, 12 N KOH and 65 °C utilizing noble metal electrocatalyst (0.5 mg platinum per cm^2 cathode, 1 mg Pd/Rh per cm^2 anode). Advanced electrodes utilizing non-noble electrocatalysts for the air cathode and 0.5 mg Pd/Rh per cm^2 for the hydrogen anode also satisfied the 2000 h operating life requirement [10]. In the present work, the degradation mechanisms of fuel cells and gas diffusion electrodes were studied in an attempt to gain the required information to further improve performance and life.

Experimental

The procedures for electrode preparation, structural analysis and fuel cell performance evaluation were reported in previous publications [5, 9, 10]. Fuel cells incorporating the described gas diffusion electrodes were assembled and operated. Changes occurring within the electrodes and the fuel cells were investigated. The scope of this work was to identify ageing and other lifetime-limiting effects to further enhance the performance and lifetime characteristics of the alkaline fuel cells and their components.

High resolution scanning (Hitachi SM-570) and transmission (Hitachi H-600) electron microscopes (SEM, TEM) were used for the morphological examinations of the electrodes and its constituents. The two instruments cover a broad range of magnification ranging from 30 times to 1.5 million times. Both instruments were equipped for access to a Kevex 8000 energy dispersive X-ray analysis system (EDX) with the capability to detect elements heavier than fluorine. A Porous Materials Inc. Autoscan automated intrusion porosimeter was available for measurements of size, distribution and the total volume of pores. This system was modified to enable the use of either mercury or an electrolyte solution as the intrusion liquid. A Quantachrome Quantasorb surface area analyzer was used for measurements of BET surface areas. The corrosion behavior of the carbon support in the electrolyte environment was determined from the heat generation in a microcalorimeter (Hart Instruments differential heat flow instrument Battery Calorimeter Model 5003) which has a peak to peak noise level of less than 0.3 μW and a precision better than 1 μW. Electron spectroscopy for chemical analysis (ESCA) spectra were collected on a PHI 5400 small spot ESCA, equipped with a dual Mg/Al X-ray source, producing incident radiation of 1253.6 eV (Mg Kα) or 1486.6 eV (Al Kα). The spectral resolution is 0.8 eV with the Mg Kα source on a Ag 3d(5/2) calibration standard [11].

Results and discussion

Electrode deterioration

Defects in the macrostructure can be introduced by deficiencies in the manufacturing process, mishandling during installation in the electrode frame, and during cell operation. Mechanical disintegration of the electrodes could be attributed to pinholes and cracks.

Chemical degradation, resulting from corrosion to various degrees of all materials used in the electrode, was observed.

Material deterioration

Carbon. X-ray fingerprinting has proven to be a valuable tool in the analysis of carbons. Figure 1 shows the X-ray energy spectroscopy (XES) spectrum for Vulcan XC 72R. Vulcan XC 72R contains high levels of sulfur, Black Pearls 2000 was found to contain relative high levels of calcium, sulfur and chlorine, whereas Shawinigan SH100 displays very low levels of inorganic contaminants. These differences are due to the raw materials and the manufacturing process used in the preparation of the carbon. Furnace Blacks (XC 2R and BP2000) mostly use oil as starting material, whereas SH100 is an acetylene black.

The X-ray photoelectron spectroscopy (XPS) spectra of Vulcan XC 72R, in the range of 0 to 1000 eV, indicate that the carbon is relatively pure and that the oxygen content is the result of oxygen containing surface groups. The sulfur (2p) spectra indicates that sulfur is present mostly in its elemental form. The elemental surface concentrations, calculated by peak integration, are 97.35% carbon, 1.32% oxygen and 1.33% sulfur. Using standard analytical techniques the sulfur content was determined to be 1.0% per bulk weight.

Depending on its chemical form sulfur can be the cause of electrocatalyst degradation/poisoning. It is therefore advisable to remove sulfur as much as possible. The extraction of sulfur was investigated using a Soxhlett extraction set-up. As expected the elemental sulfur present in the carbons can be removed substantially by solvents for sulfur (Table 1). Nitric acid and water extraction significantly reduce calcium, chlorine and silicon levels of the carbon. All treatments (except for the nitric acid were found not to significantly affect the surface area of the carbon. It was observed that the wetting characteristics of the carbon were affected by the extraction. For example, the contact angle for the CCl_4 treated sample was 152° as compared with 148° for the untreated material, as determined by a Quantachrome mercury contact

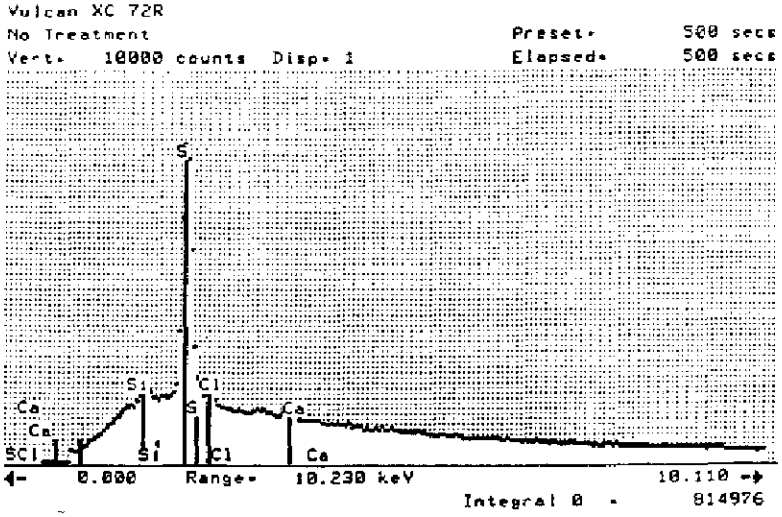

Fig. 1. XES spectrum of Vulcan XC 72R revealing the inorganic contaminants.

TABLE 1

The effect of methods of extraction over 17 h by various fluids on the sulfur content of Vulcan XC 72R

Extraction fluid	Extraction temperature	Sulfur content (%)
None		1.00
Isopropylalcohol	82	0.77
Acetone	56	0.72
Water	100	0.63
Toluene	110	0.61
Nitric acid	20	0.21

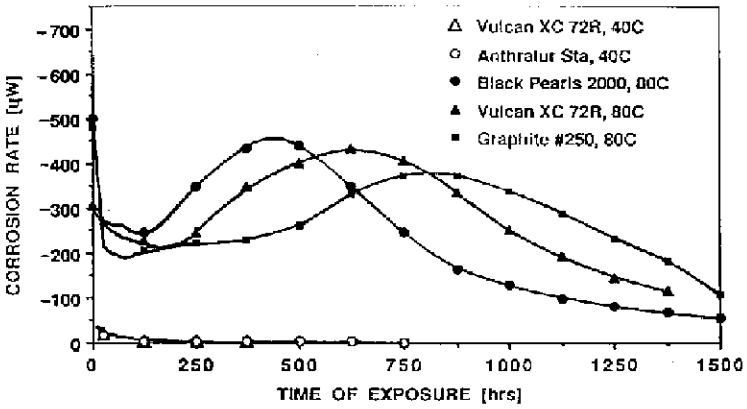

Fig. 2. Corrosion rates of Black Pearls 2000, Vulcan XC 72R, Micro #250 graphite at 80 °C and Vulcan XC 72R and Anthralur Sta at 40 °C determined by microcalorimetry (sample size: 0.5 g carbon).

angle analyzer. An alternate sulfur removal technique is heat treatment of the carbon above 1600 °C.

The stability of carbon materials against chemical attack is paramount for long life expectancy in AFCs. Earlier microcalorimetric investigations revealed that various carbon materials display different corrosion rates [12]. The addition of electrolyte increases the corrosion rate drastically, KOH having a more pronounced effect than phosphoric acid at the same temperature. The addition of platinum (1 mg/g carbon) was found to drastically increase the corrosion rate during the first 50 h; the carbon corrosion rate levels off faster in the presence of the noble metal, and remains at higher levels than without the noble metal addition. These observations confirm that the noble metal acts as a carbon corrosion catalyst. Figure 2 shows the long-term corrosion rate of Black Pearls 2000, graphite micro #250 and Vulcan XC 72R in 12 N KOH at 80 °C over 1500 h. The corrosion behavior first levels off within the first 200 h indicating that the outer surface is wetted. The rapid increase in the corrosion rate after 500 h could be due to the fact that electrolyte starts to penetrate and corrode the inside of the carbon agglomerates. Such a behavior is not observed for as long as 1500 h of exposure at 40 °C. After about 1000 h at 80 °C, carbon corrosion again starts to level off. The structure of the original and the corroded

Vulcan XC 72R carbon was determined by transmission electron microscope (TEM). Analyzing Vulcan XC 72R exposed to 12 N KOH at 80 °C for 2300 h, it appears that the smaller particles have been totally oxidized, and the bigger particles have been reduced in size. As a result the particles size distribution of the corroded carbon is much narrower than the one of the original material. The BET surface area of the Vulcan XC 72R was found to have reduced from 225 to 125 m^2/g. In a fuel cell electrode, the rate of this corrosion process can vary. It can be significantly delayed by the presence of PTFE and the possible liquid wetproofing treatment or accelerated by the presence of peroxide.

Polytetrafluoroethylene. PTFE is a hydrophobic, chemically-stable, plastic material used as a binder for different types of carbon to create a porous electrode structure [13]. Electrodes can be made from two types of PTFE, and aqueous suspension and a dry powder. Surface properties of PTFE are altered by exposure to KOH electrolyte, as revealed by the decreased contact angle and hence of the surface tension. Further, SEM examination of the PTFE surfaces reveals a roughening of the surface caused by KOH electrolyte. These changes were shown to depend on the types and particle sizes of PTFE. Thus, changes occurring to the PTFE under fuel cell operating conditions can also contribute to the electrode degradation, e.g., increased flooding. In fuel cells chemical degradation of the PTFE can also be caused by the access of the electrolyte and accelerated by the presence of peroxide.

Electrocatalyst. It has been shown that exposure of platinum on carbon or water or phosphoric acid over a period of 200 h does not result in any noticeable changes of the platinum crystallites size (30 Å) [14]. However, exposure to KOH results in an increase of the platinum particle size from 30 to 100 Å within hours of exposure. At a loading of 0.5 mg platinum/cm^2 no performance degradation is observed in AFC indicating that the platinum agglomeration to 100 Å does not alter the electrode performance.

KOH exposure to platinum supported carbon catalyst (Prototech) was found to have a drastic effect on the noble metal. Agglomeration of platinum particles was observed to start as soon as the samples were exposed to KOH and the size of the agglomerates seemed to increase logarithmically over a period of 48 h. Within this time the particle size was found to increase from less than 50 to over 200 Å. Some small particles were still observed but their number significantly decreased with increasing time of exposure. No attempt was made to study the influence of platinum agglomeration on performance at loadings lower than 0.5 mg/cm^2.

Current collector. Both the edge collected and bipolar construction method were evaluated. Nickel and silver were found to be suitable metallic current collectors for use in edge collected AFCs. Metal screens, perforated plates, porous plaques and fibrous mats are commercially available. The anode current collector is maintained at a potential, sufficiently negative that the metallic surface of e.g. the nickel is maintained. In the case of the cathode current collector, however, it was found that at the operating potentials of the air cathode a nickel oxide film, established on the nickel surface within a few days, increased the contact resistance between the PTFE/carbon layer and the current collector, even when the nickel screen was embedded on the gas side and separated from the active layer by a highly hydrophobic gas diffusion layer. Changing the cathode current collector to silver or silver plating of the nickel current collector was found to be effective in preventing metal current collector oxidation. Silver only forms oxides at relatively high potentials. In addition silver oxides exhibit a high degree of conductivity. Carbon/graphite coatings (e.g., Electrodag TM) were also successfully employed. For cathodes operating at current densities in excess of 150 mA/cm^2 on

oxygen, a thin layer of gold coating on the surface of the current collector was found to be beneficial in minimizing the internal resistance drop.

When a bipolar current collector is used, the critical task is to minimize the contact resistance between the bipolar plate and the carbon electrode. Proper surface preparation methods are essential. Combinations of sandblasting, followed by chromic acid etching of the bipolar plate to remove the surface plastic and expose the conductive carbon/graphite/graphite fiber and were found to be suitable pretreatments. Care has to be taken in the preparation of the gas diffusion layer that no PTFE film is present on the surface to avoid any contact resistance. Methods, investigated to achieve a good electrical contact between the bipolar plate and the carbon electrode, include pressure contact and adhesive and heat-welding techniques. Pressure contacts maintained typically by spacers acting as springs in the electrolyte compartment or application of electrolyte overpressure, are highly unreliable and were found to degrade quickly. Adhesive techniques produced reliable electrical contacts in particular when a metal filler (e.g., conductive silver epoxy) was used or when an adhesive without a conductive additive was applied in a manner that the conductive contact between the bipolar plate and the carbon electrode was maintained. Attachment of the carbon electrode to the bipolar plate by heat-welding is another viable alternative. Care has to be taken to avoid melting, as otherwise a plastic film forms on the surface of the bipolar plate.

Electrode degradation

Electrode degradation is caused by breakdown of macro- and microstructures. Macrostructure defects are frequently associated with structural deficiencies. Electrode microstructure defects are typically associated with carbon corrosion and loss of electrocatalytic activity. Pinholes as shown in Fig. 3 frequently are the result of inhomogeneous carbon/PTFE pastes (e.g., failure to break agglomerates of carbon and/or solid filler) and cause leakage of electrolyte to the gas side. Cracks, as shown in Fig. 4, are frequently introduced during manufacture (e.g., by accelerated drying which results in 'mud-cracking') or mishandling during installation of the electrodes in the fuel cell. In addition, cracks can be caused by stresses generated during temperature cycling (e.g., if the two carbon layers are not properly matched in thermal expansion). During operation, the exposure of electrodes to the electrolyte can result in swelling (in particular of the catalyst layer, e.g., if the carbons have not been subjected to an appropriate pretreatment) causing cracks or potentially delamination.

With ageing, increased wetting of the gas diffusion layer is observed. The result is a decline of peak power performance due to reduced gas transport which becomes apparent in particular in cathodes operating on air and further lead to electrolyte weepage to the gas side.

Table 2 shows the effect of macrostructure wetting in the diffusion layer of electrodes optimized for operation in AFCs and for commercially-available phosphoric acid fuel cell (PAFC) electrodes, comprising a catalyst layer and a highly-teflonized carbon paper backing (Stackpole PC206). The oxygen electrode behavior on these electrodes showed that the electrocatalyst and the electrocatalyst layers performed satisfactorily. However, when operated with 50 and 20% oxygen, despite the higher porosity and hydrophobicity (50% PTFE, Fig. 5) of the carbon paper backing (typically used in PAFC electrodes), the KOH electrolyte penetrates the diffusion layer and prevents sufficient gas transport to support the oxygen reduction. A properly designed diffusion layer (Fig. 6) maintains excellent operating characteristics, despite the low PTFE (35%) content and the reduced porosity.

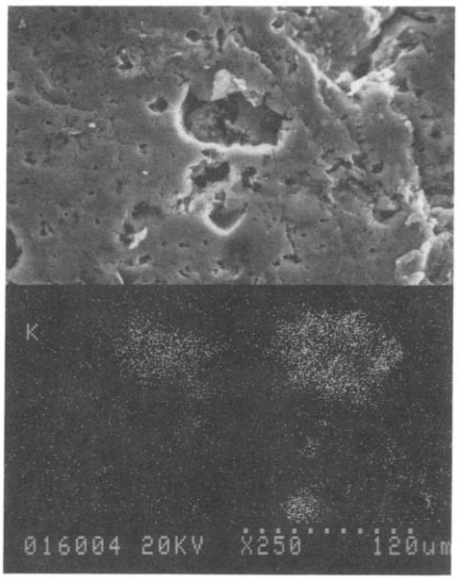

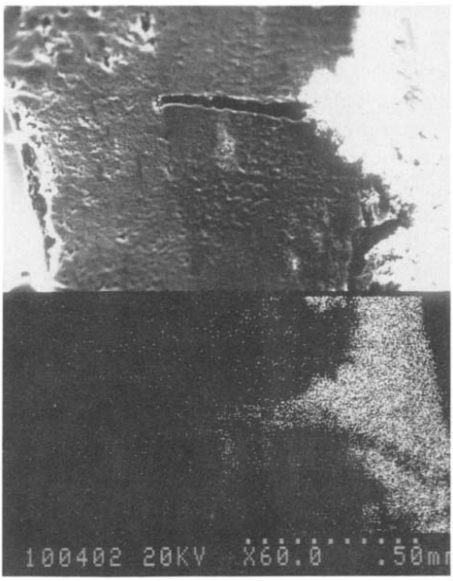

Fig. 3. Split screen image of the gas diffusion side of an air electrode after operation of 507 h on air at 100 mA/cm^2 at 65 °C in 12 N KOH electrolyte. The upper portion represents the SEM picture. The lower one the XES tracing for potassium revealing KOH electrolyte weapage through pinholes of the electrode.

Fig. 4. Split screen image of an air electrode cross section after operation of 217 h on air at 100 mA/cm^2 at 65 °C in 12 N KOH electrolyte. The upper portion shows the SEM picture. The lower one the XES tracing for potassium. The crack in the catalyst layer which has been flooded by the KOH electrolyte is revealed.

TABLE 2

Electrode performance of various types of electrodes at various oxygen partial pressure after operation for approximately 200 h in 12 N KOH at 65 °C at 100 mA/cm^2 with air

Electrode (operating time at 100 mA/cm^2)	Current density (mA/cm^2)	Potential (mV vs. RHE)		
		100% O_2	50% O_2	20% O_2
B502 AFC, 200 h	100	910	900	850
	200	900	880	820
	300	900	875	750
Westinghouse PAFC, 172 h	100	950	950	890
	200	950	930	750
	300	940	920	<500
Prototech PAFC, 175 h	100	910	890	600
	200	900	850	<500
	300	890	820	<500

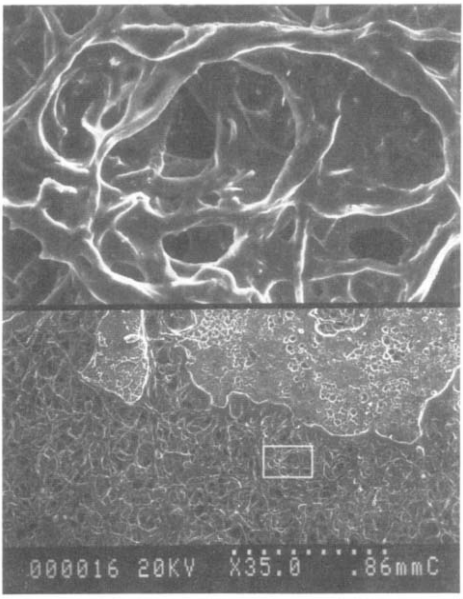

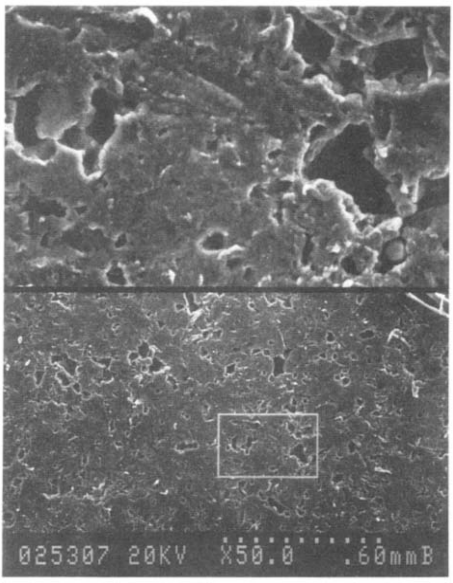

Fig. 5. Split screen SEM picture of a porous carbon paper backing (Stackpole PC206) as used in PAFC fuel cells. The upper part shows the rectangular section marked at 10× the magnification.

Fig. 6. Split screen SEM picture of a carbon/PTFE gas diffusion layer optimized for AFC use. The upper part shows the rectangular section marked at 5× the magnification.

Degradation phenomena due to fuel cell operation

Electrodes

To study degradation phenomena occurring in AFC electrodes during operation 100 cm^2 active area, single and multicell stacks were assembled and operated. Performance and life-limiting factors were studied. Additional complications arose during fuel cell stack operation, due to inhomogeneous current density distribution and uneven reactant gas feed within the individual cells and the fuel cell stack. To study cell operation effects, test electrodes were removed from operating fuel cells at various times and exposed to ESCA analysis. The resulting spectra were compared to the ones obtained with unused electrodes. Figures 7 and 8 compare the ESCA survey spectra of a new cathode and a cathode operated successfully in a fuel cell for 430 h at 100 mA/cm^2 in 12 N KOH at 65 °C. Table 3 summarizes the elemental analysis data obtained and in addition lists the composition of the electrocatalyst used in air electrodes. The overall carbon content remained virtually unchanged. This is to be expected as any oxidation products of the carbon corrosion tend to precipitate within the electrode. The C(1s) spectra of the cathodes are shown in Fig. 9. It can be seen that the oxygen content of the air electrodes increases significantly during operation, which is due to carbon corrosion.

O(1s) spectra of cathodes (Fig. 10) are characteristic of metal oxide, probably from the oxide layer on the noble metal electrocatalysts. These oxides are present whenever electrode samples are exposed to air. The decrease in fluorine content indicates that PTFE does degrade under conditions exposed to in an AFC. The XPS F(1s) spectra for AFC electrodes (Fig. 11) contain further evidence of PTFE degradation. The increase in the peak width towards higher binding energies indicates that the

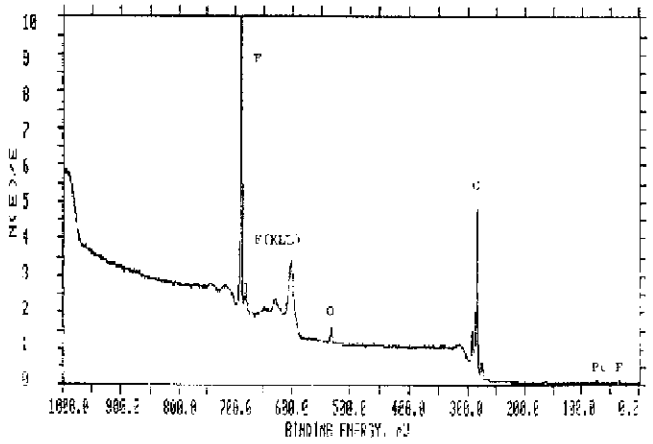

Fig. 7. ESCA survey spectra of an unused air cathode containing 0.5 mg/cm² Pt. T = 9.33 min, Mg 300 W, pass energy = 44.75 eV, scale factor, offset = 21.898, 1.350 kcounts/s, exit angle = 45°.

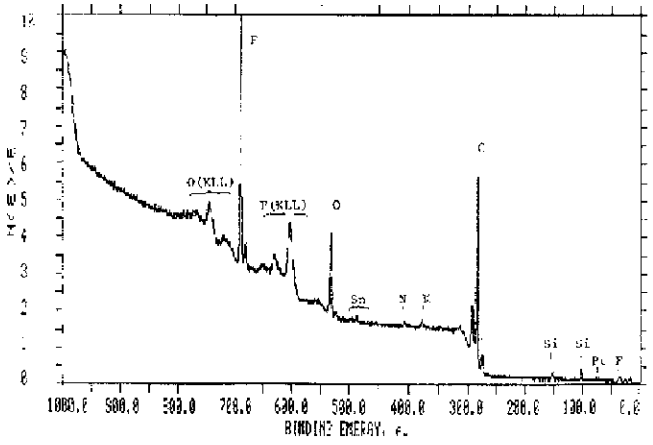

Fig. 8. ESCA survey spectra of an air cathode after 430 h of operation at 100 mA/cm² at 65 °C in 12 N KOH. T = 9.33 min, Mg 300 W, pass energy = 44.75 eV, scale factor, offset = 11.803, 1.189 kcounts/s, exit angle = 45°.

chemical environment of the fluorine atoms has changed to one having more electronegative nearest neighbors. It can be expected that the electronegativity of the PTFE carbon chain increases during oxidative additions of functional groups containing, e.g., oxygen, nitrogen or chlorine. In addition to this observed chemical environment change, quantitative loss of PTFE is suggested by a significant decrease in the F(1s) (Fig. 11) and the C(1s) (Fig. 9) fluorocarbon signals. The increase in the oxygen content due to corrosion and the increased PTFE degradation manifest themselves in a loss of hydrophobicity resulting in increased electrolyte uptake. The platinum content has not changed significantly over the 430 h of operation, however, a shift to a higher oxidation state was observed on the electrode. The Pt(4f) peaks are indicative of oxide covered metal in the cathodes (Fig. 12). In cells having operated in excess of 1000 h under similar conditions some loss of platinum from the cathode

TABLE 3

Elementary analysis (in atomic percent) of various air cathodes and 10% Pt/carbon using ESCA

Element	Cathode					
	Unused		430 h operation		Prototech (10% Pt/C)	
	At.%	At ratio to C×100	At.%	At ratio to C×100	At.%	At ratio to C×100
Carbon	64.46	100.00	63.38	100.00	93.18	100.00
Oxygen	3.09	4.79	11.95	18.85	4.27	4.58
Sulfur	0.53	0.82	0.51	0.80	0.97	1.04
Platinum	0.12	0.19	0.09	0.14	1.58	1.70
	(3.02 wt.%)		(2.30 wt.%)		(27.09 wt.%)	
Fluorine	31.25	48.48	19.90	31.40		
Nitrogen	0.56	0.87	0.65	1.03		
Silicon			3.36	5.30		
Tin			0.65	1.03		

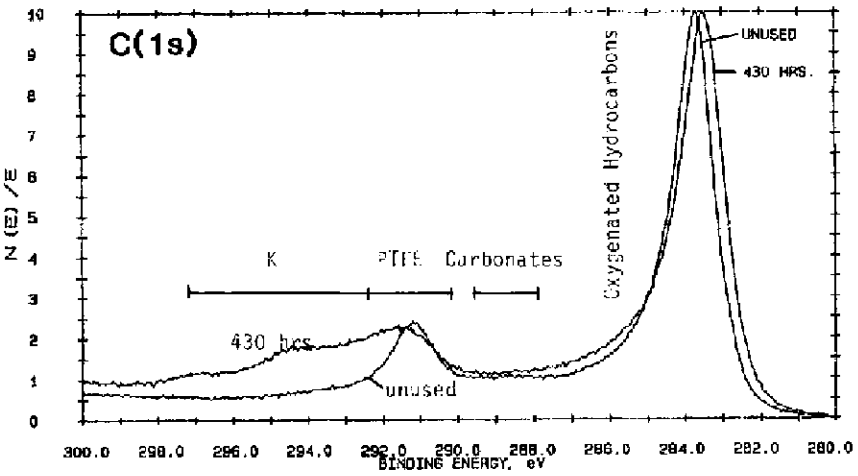

Fig. 9. C(1s) photoelectron spectra of AFC air cathodes using Mg Kα X-radiation (1253.6 eV).

was observed as well. Life-limiting effects of the cathode can be mostly attributed to carbon corrosion and loss of hydrophobicity resulting in partial flooding and plugging of the pore structure limiting mass transport. A slow deterioration of air cathodes (10 to 30 mV/1000 h at 100 mA/cm^2) could be due to carbon corrosion and electrocatalyst degradation. Catastrophic electrode failures were caused by cracks and delamination caused by swelling. Figures 13 and 14 and Table 4 compare the ESCA spectra of a new and a prematurely failed anode. C(1s) spectra of anodes (Fig. 15) show a shift of 2.5 eV for the used versus unused anode. This is reasonable evidence of elemental carbon reacting to form non-volatile and insoluble hydrocarbons with oxygenated side groups like hydroxyl, ketone, aldehyde, ether and ester groups. It is not possible to extract a precise identification of the carbon degradation end products, but ESCA

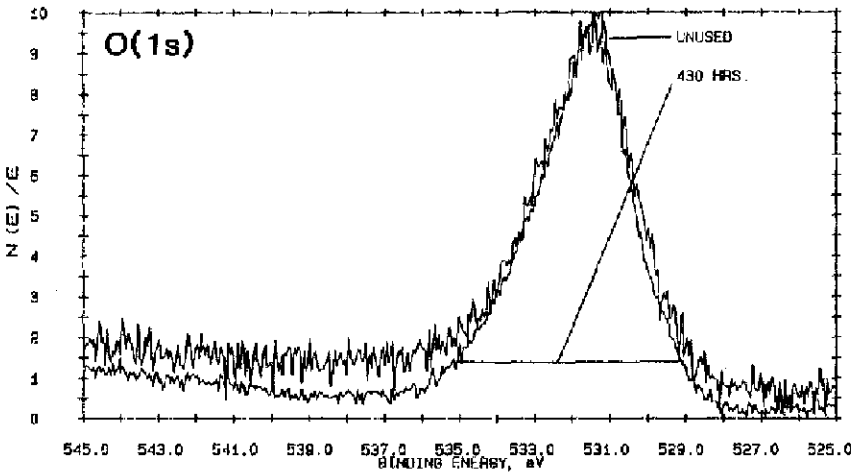

Fig. 10. O(1s) photoelectron spectra of AFC air cathodes using Mg Kα X-radiation (1253.6 eV).

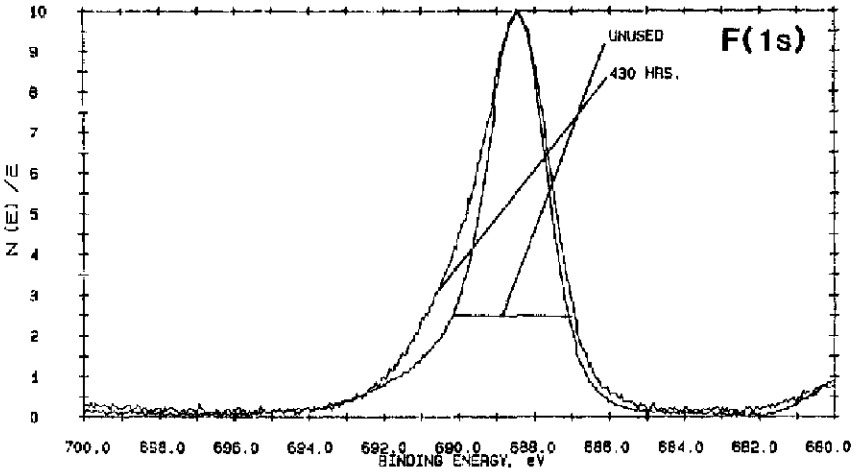

Fig. 11. F(1s) photoelectron spectra of AFC air cathodes using Mg Kα X-radiation (1253.6 eV).

clearly demonstrates a significant change in the carbon chemical environment in the failed anode. Figure 16 shows the O(1s) spectra of the various anode samples. The O(1s) peaks of a new AFC anode shows broad spectra due to nitrates and oxides (unused electrode) and oxides and KOH (50 h). The oxygen content of the unused anode originates from the noble metal salts (nitrates) used during electrocatalyst deposition. In contrast to the anode, the source of oxygen in the cathodes could be attributed to functional groups on the carbon. These observations can be explained on the basis of the method used for fabrication of anodes [10, 15]. Hydrogen electrodes are fabricated without any electrocatalyst, the electrodes are postcatalyzed by brushing on an alcoholic solution containing the noble metal salts. The reduction of the noble metal salts occurs merely when the electrodes are placed in fuel cells and exposed to hydrogen and electrolyte during the break in procedure. The O(1s) spectrum for

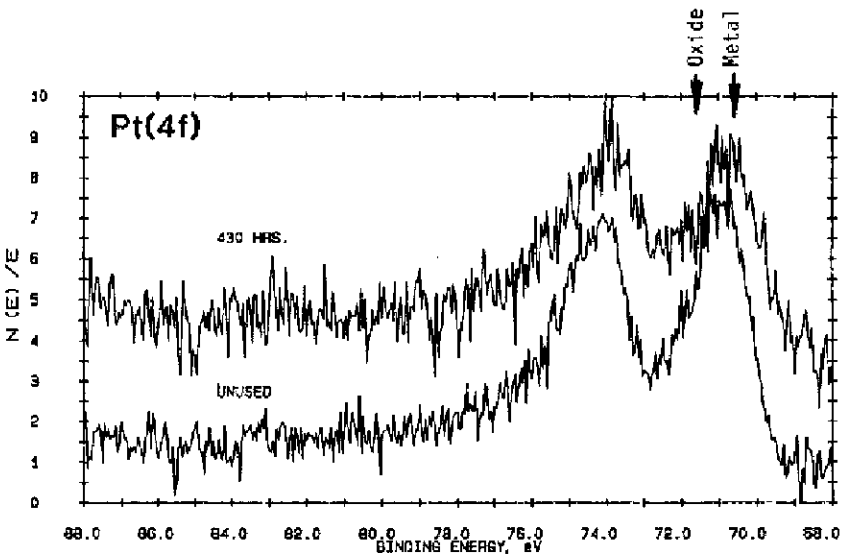

Fig. 12. Pt(4f) photoelectron spectra of AFC air cathodes using Mg Kα X-radiation (1253.6 eV).

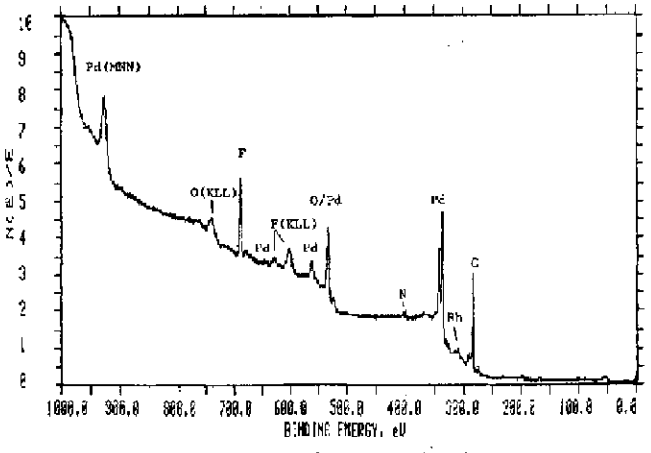

Fig. 13. ESCA survey spectra of an unused hydrogen anode containing 1 mg/cm^2 Pd/Rh. T = 9.33 min, Mg 300 W, pass energy = 44.75 eV, scale factor, offset = 21.679, 4.139 kcounts/s, exit angle = 45°.

the failed anode shows a shift towards higher binding energies, which is also consistent with the expected behavior of oxygenated hydrocarbons. This evidence is consistent with the operating mode of the electrodes. The tests cells are operated at constant current and a hydrogen electrode unable to maintain hydrogen oxidation at 100 mA/cm^2 will eventually operate in the oxygen evolution mode. PTFE degradation has been confirmed (Fig. 17), sulfur and chlorine impurities leached out during the 713 h of operation.

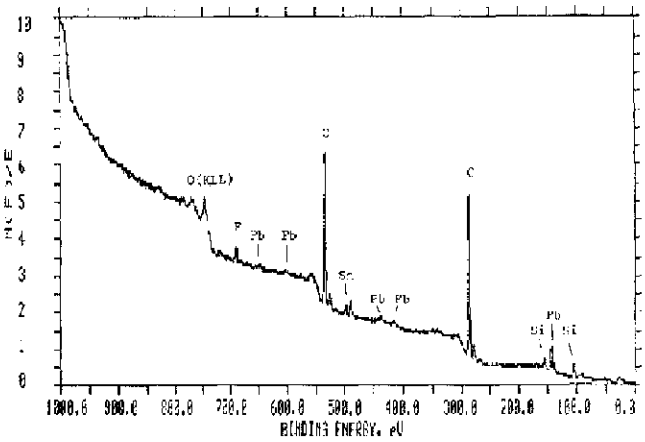

Fig. 14. ESCA survey spectra of a hydrogen anode which failed prematurely after 713 h of operation due to catalyst poisoning by lead and tin impurities at 100 mA/cm^2 at 65 °C in 12 N KOH. T=9.33 min, Mg 300 W, pass energy=44.75 eV, scale factor, offset=14.183, 1.214 kcounts/s, exit angle=45°.

TABLE 4

Elementary analysis (in atomic percent) of various hydrogen anodes using ESCA

Element	Anode					
	unused		50 h operation		713 h failed	
	At.%	At ratio to C×100	At.%	At ratio to C×100	At.%	At ratio to C×100
Carbon	47.33	100.00	67.13	100.00	65.78	100.00
Oxygen	27.45	58.00	17.20	25.62	63.78	36.15
Sulfur	0.96	2.03	0.70	1.04	0.74	1.12
Fluorine	12.95	27.36	11.14	16.59	1.88	2.86
Nitrogen	3.39	7.16	0.96	1.43	0.64	0.97
Chlorine	1.08	2.28	1.20	1.79	0.16	0.24
Palladium	6.51	13.75	1.08	1.61	0.23	0.35
Rhodium	0.33	0.70	0.59	0.88		
Silicon					5.78	8.79
Tin					0.41	0.62
Lead					0.61	0.93

The Pd in the anode is clearly in a high oxidation state in the unused form. The ESCA spectra shows a metallic component after 50 h of operation indicating that the noble metal reduction is occurring during early cell operation (Fig. 18). The failed anode shows virtually a total removal of catalyst (Figs. 18 and 19), with only a very weak metallic signal remaining. The Rh(3d) region for the 50 h anode shows that this element is in an oxidized state. The oxide was probably too thick to be reduced during operation. At an overpotential of 200 mV versus reversible hydrogen electrode (RHE) palladium and rhodium were found to form oxides which partly dissolve. The

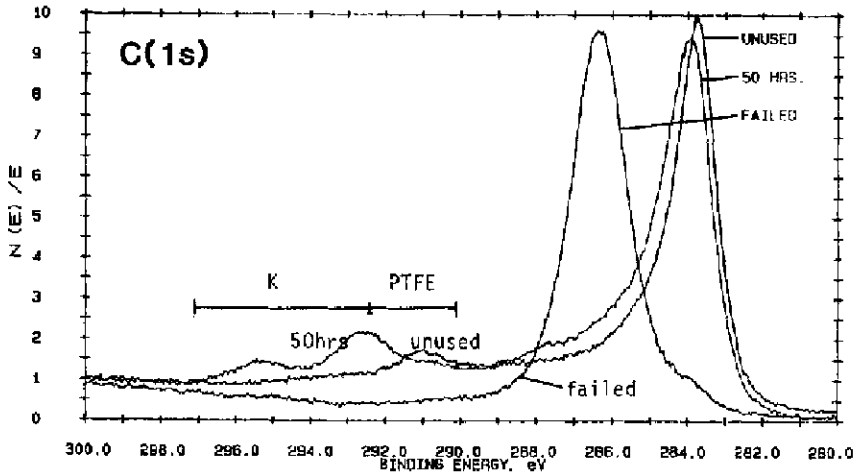

Fig. 15. C(1) photoelectron spectra of AFC hydrogen anodes using Mg Kα X-radiation (1253.6 eV).

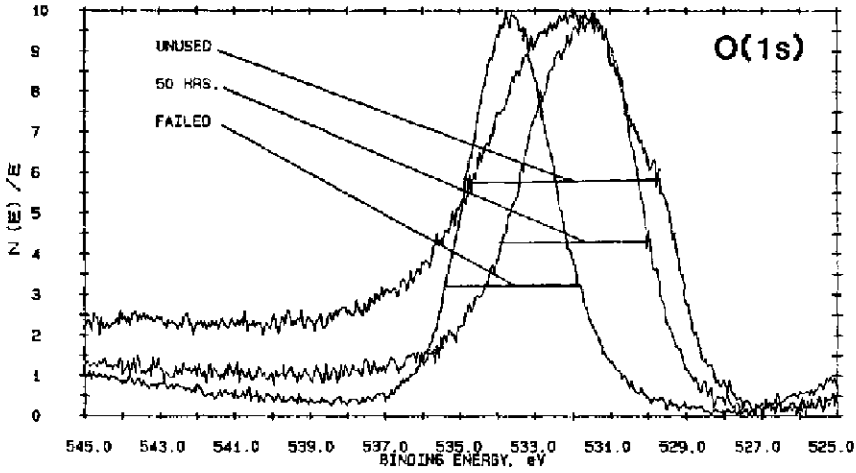

Fig. 16. O(1s) photoelectron spectra of AFC hydrogen anodes using Mg Kα X-radiation (1253.6 eV).

dissolved electrocatalyst from the anode was found to plate out in the electrolyte loop. During cell operation, lead and tin impurities were leached out from various AFC components by the electrolyte and were found to deposit on the anode. These tin and lead deposits are probably responsible for the electrocatalyst poisoning resulting in hydrogen electrode failure. The origin of the impurities were determined. Silicon originated from grease, tin from solder, and lead leached out from solder or glass components. The predominant cause for premature hydrogen electrode failure is thus electrocatalyst poisoning.

Internal resistance effects

Figures 20 and 21 show the electrical performance of a 100 cm^2 active area AFC over 1000 h of operation. Figure 22 shows the cell design. The bipolar plate contained

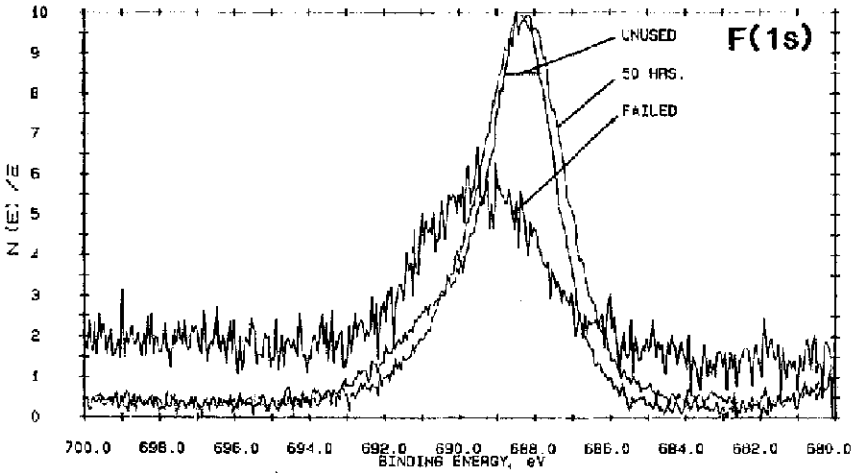

Fig. 17. F(1s) photoelectron spectra of AFC hydrogen anodes using Mg Kα X-radiation (1253.6 eV).

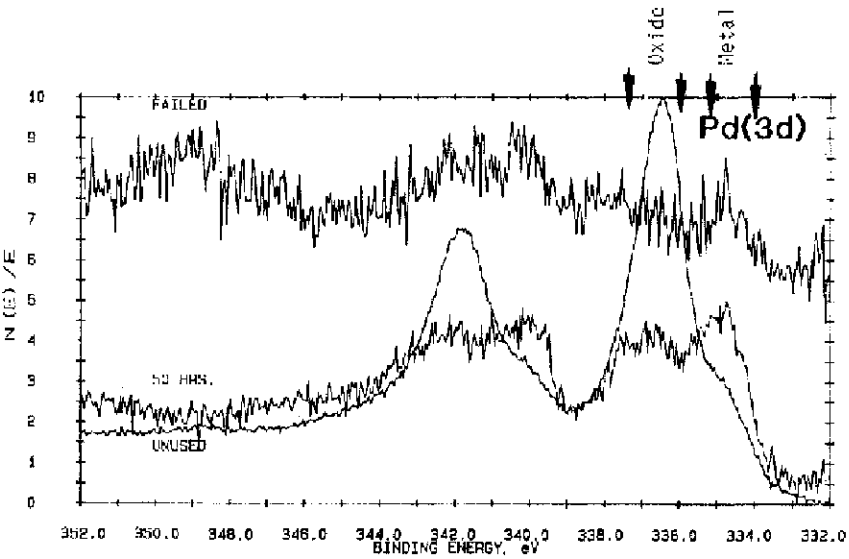

Fig. 18. Pd(3d) photoelectron spectra of AFC hydrogen anodes using Mg Kα X-radiation (1253.6 eV).

SX.1, a carbon-filled conductive plastic which was nickel-plated on both sides; the electrodes utilized a carbon cloth backing and were attached to the bipolar plate by silver epoxy. The increase in internal resistance between cathode and the bipolar plate demonstrates that a nickel contact surface is unacceptable. The cell was operated at 65 °C for the first 50 h. Between 50 and 300 h it was operated at 20 °C. After 400 h the electrolyte-feeding channels were plugged with debris, shedding from the electrodes and required cleaning. At this point the operating temperature was increased to 65 °C and maintained for the remainder of the test. Figure 21 demonstrates the

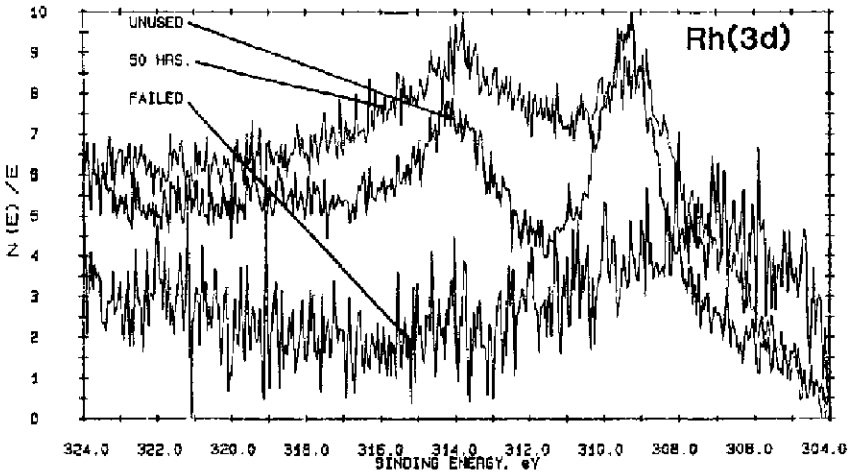

Fig. 19. Rh(3d) photoelectron spectra of AFC hydrogen anodes using Mg Kα X-radiation (1253.6 eV).

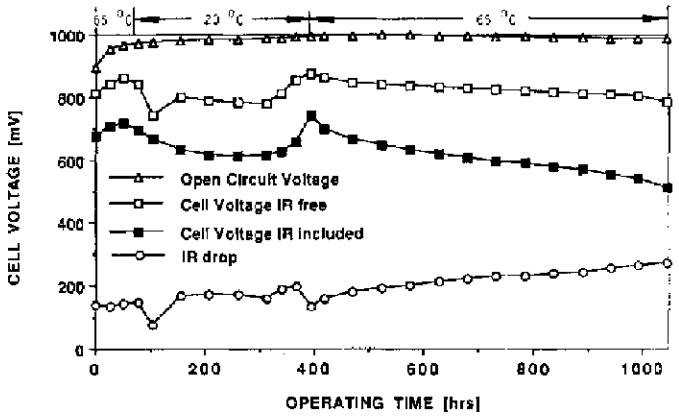

Fig. 20. Performance of a 100 cm^2 AFC over a period of 1000 h at 100 mA/cm^2.

increase in internal resistance of the cathode and the cathode to bipolar plate contact appeared to limit the performance of the cell. As a consequence, nickel components used on the cathode side were replaced by silver resulting in lowering of the internal resistance over the lifetime of the AFC (Fig. 23). The successful operation of AFCs with low internal resistance losses, even at high operating current densities, is demonstrated in Fig. 24.

Mechanical effects

A series of temperature cycle experiments with both edge collected and bipolar electrode plate subassemblies were carried out to obtain an insight into the problem of electrode buckling and the quality of the electrical contact between plate and electrode. Attaching a nickel screen to the bipolar plate and subjecting the screen/

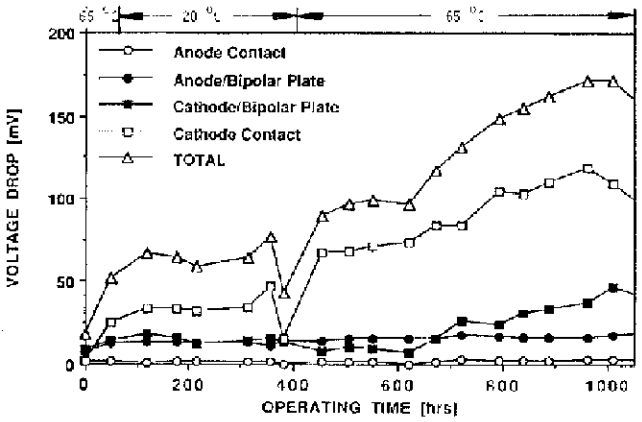

Fig. 21. The change of AFC components internal resistance of a 100 cm^2 AFC over a period of 1000 h at 100 mA/cm^2.

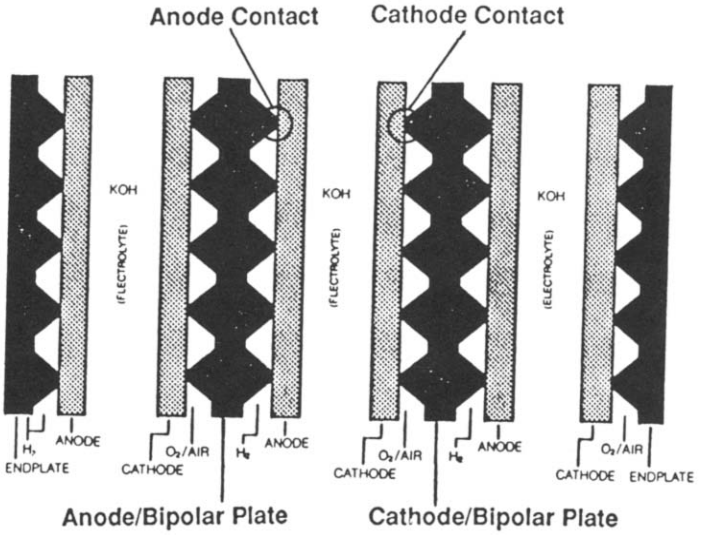

Fig. 22. Schematic of a bipolar AFC as used in the program.

bipolar plate assembly to temperature cycles between 20 and 80 °C caused stretching and buckling in the first few cycles. This indicates that the nickel screen was stretched beyond its elastic deformation limit. A screen coupled with the polypropylene/carbon plate resulted in plastic deformation and buckling when the temperature swing exceeded 30 °C. Similar problems were observed by embedding nickel screens in PTFE bonded carbon electrodes and subjecting them to the same temperature changes. Electrode substrates like carbon cloth were determined to be significantly better matched to the bipolar plate in respect to compatible thermal expansion.

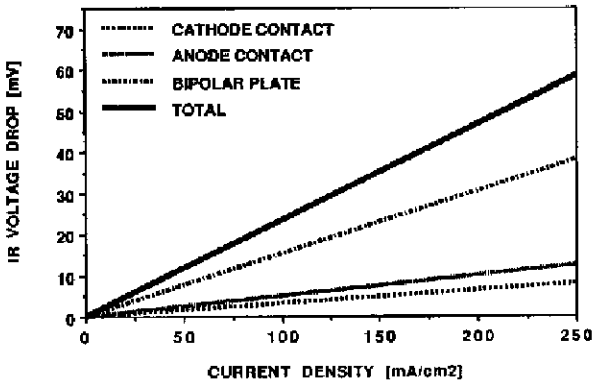

Fig. 23. Internal resistance losses occurring in an AFC bipolar plate assembly as a function of the current density at 65 °C using SX.1 bipolar plates, silver cathode contacts, nickels anode contacts and conductive epoxy to attach the electrodes to the bipolar plates.

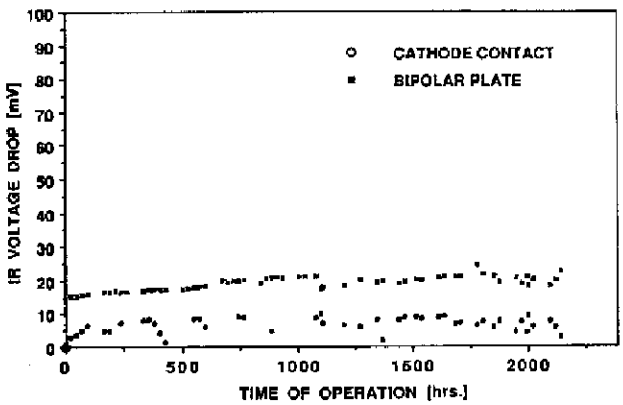

Fig. 24. Internal resistance components on the cathode side of a silver plated bipolar plate in an AFC operating at 100 mA/cm^2 on air at 65 °C.

Conclusions

The use of state-of-the-art equipment in the characterization of AFCs and their components was successfully demonstrated. SEM and TEM with XES on electrodes and electrode materials were found to provide useful information about the initial structure of electrodes and electrode materials and clearly reveal the changes occurring during the service life of AFCs. XES revealed useful information on electrolyte penetration and catalyst distribution during AFC operation. Intrusion porosimetry provided information on the pore structure and the surface area of electrodes and active materials. Microcalorimetry was used to study stability of active materials in particular carbon as a function of the temperature and the operating time. The usefulness of ESCA as a surface technique to provide more sensitive information than 'bulk' methods was demonstrated. Failures of the primary electrode structure (cracks, delamination) frequently cause premature electrode failure. Degradation effects of the secondary electrode structure include corrosion of virtually all materials. Generally

failures of the secondary electrode structure results in a slow degradation of the electrochemical performance of the electrode with increasing operating time.

In air electrodes, carbon is slowly oxidized resulting in the introduction of functional oxygen groups. One consequence of the carbon corrosion is an increase in wetting by the KOH electrolyte, resulting in increased electrolyte penetration causing internal flooding. Gas transport is the performance-limiting factor and peak power performance with air as reactant degrades while electrodes are still capable of operation at high-current densities with pure oxygen. Further improvements in the stability of carbon materials seems necessary to significantly prolong the lifetime of air electrodes in alkaline electrolyte fuel cells. Carbon pretreatments such as heat activation [16], fluorination [17] and Nafion impregnation [18] need to be further pursued. PTFE degradation also, results in decreased hydrophobicity and an increased electrolyte uptake further reducing the pore system available for gas transport. The agglomeration of platinum crystallites in KOH electrolyte was identified to occur quite early in the electrode wet-life; however, at the level of noble metal loadings employed, the electrocatalyst was not a lifetime-limiting factor.

In the case of the hydrogen anodes the partial conversion of carbon to hydrocarbon compounds was verified using ESCA. PTFE degradation in anodes too, was confirmed. Anode failures are attributed to electrocatalyst problems frequently associated with impurities, from AFCs extracted by the electrolyte and their subsequent deposition on the anode catalyst layer. Improvements desired in anode electrocatalysis include enhanced performance at reduced noble metal loadings and an increased tolerance to impurities. The proper choice of cell materials and cell design are also critical issues in achieving increased lifetimes with AFCs.

The increase in internal resistance of AFCs with operating time could be attributed to the degradation of the contact between the bipolar plate and the electrodes as well as that between the metal current collector and the carbon layer, particularly in air cathodes operating at high potentials. The replacement of nickel with silver or carbon structures were found to remedy this problem.

Other problems observed with AFC electrodes include mechanical problems caused by mismatched coefficients of thermal expansion of the various cell components resulting in a sensitivity to temperature cycling. Carefully-addressing parameters identified to be responsible for the performance and lifetime limitations experienced with AFCs, should further enhance the potential for developing such types of low-cost, high-performance fuel cell powerplants.

Acknowledgement

This work was funded by the Ontario Ministry of Energy (OMENG). Permission given by Battery Technologies Inc. to release the paper for publication is appreciated.

References

1 K. Kordesch and J. Oliveira, Fuel Cells, *Ullmann's encyclopedia of industrial chemistry, 5th edn, VCH Verlagsgesellschaft MbH, Weinheim, 1989, pp. 55–83.*
2 Elenco NV, *Fuel Cell Brochure,* Dessel, Belgium, 1990.
3 A. Emery, Oxy-hydrogen-air fuel cell, *Fuel Cell Seminar, Orlando, FL, USA, Nov. 13–16, 1983,* Abstr., pp. 98–102.

4 D. W. Sheibley, J. D. Denais and L. S. Murgia, NASA fuel cell applications for space, *National Fuel Cell Seminar, Orlando, FL, Nov. 13–16, 1983*, Abstr., pp. 107–110.
5 F. Baron, European activities on fuel cells for space, *Fuel Cell Seminar, Long Beach, CA, Oct. 23–26, 1988*, Abstr., pp. 255–162.
6 K. Tomantschger, F. McClusky, L. Oporto, A. Reid and K. Kordesch, *J. Power Sources, 18* (1986) 317–335.
7 K. Kordesch, J. Gsellmann, R. Findlay, S. Srinivasan and K. Tomantschger, Electrode design and concepts for bipolar, alkaline fuel cells, *Hydrogen Energy V, Proc. 5th World Hydrogen Conf., Toronto, Ont, July 15–20, 1984*, Vol. 4, pp. 1657–1668.
8 K. Kordesch, J. Gsellmann, S. Jahangir and M. Schautz, The technology of PTFE-bonded carbon electrodes, *Proc. Symp. on Porous Electrodes Theory and Practice, Electroch. Soc. Inc., Pennington, NJ*, Vol. 84-4, pp. 163–190.
9 K. Tomantschger and K. Kordesch, *J. Power Sources, 25* (1989) 195–214.
10 K. Tomantschger, F. McClusky, L. Oporto, A. Reid and K. Kordesch, *Performance Evaluation of the Institute for Hydrogen Systems Porous Gas Diffusion Electrodes, IHS Report*, Mississauga, Ont., 1986.
11 C. D. Wagner, W. M. Riggs, L. E. Davis, J. F. Moulder and G. E. Muilenberg (eds.), *PHI Handbook of X-ray Spectroscopy*, Perkin Elmer Corporation, Eden Prairie, MI, 1979.
12 K. Tomantschger, Investigations of Electrodes and Electrode Materials Used in Electrochemical Power Sources Considered for Hybrid Electric Transportation Systems, *PhD Thesis*, Technical University Graz, 1981.
13 K. Kordesch, *Fuel Cells*, Springer, New York, 1984.
14 L. Pataki, R. D. Venter, A. D. Reid, C. J. Maggiore and S. Srinivasan, Effects of the electrolyte temperature and CO treatment on stability of fuel cell platinum electrocatalyst, *Electrochemical Soc. Meet., Toronto, Ont., May 12–17, 1985*, Ext. Abstr. no. 659, pp. 924–925.
15 K. Tomantschger and L. Oporto, *Fabrication Procedures for the IHS Porous Gas Diffusion Electrodes, IHS Report*, Mississauga, Ont., 1985.
16 K. Tomantschger, K. Kordesch and R. Findlay, *US Patent 5 069 988* (1992).
17 N. Weinberg, *US Patent 4 908 198* (1990).
18 E. Solomon, Y. Genodman and J. Irizarry, *US Patent 4 877 694* (1989).